THE JOURNAL OF PHYSICAL CHEMISTRY B

Article

pubs.acs.org/JPCB

A- to B-Form Transition in DNA Between Gold Surfaces

One-Sun Lee, Vince Y. Cho, and George C. Schatz*

Department of Chemistry, Northwestern University, 2145 Sheridan Road, Evanston, Illinois 60208-3113, United States

ABSTRACT: Molecular dynamics simulations have been performed to characterize the conformation of DNA that is present when DNA links gold nanoparticles to form nanoparticle superlattice crystals. To model the DNA-linked gold nanoparticles, four strands of DNA are used to connect two gold surfaces, with a small interstrand separation and high added salt to match experiment. A-form DNA was assumed for the initial conformation, as this form of DNA has a length per base-pair that matches lengths that have been inferred from X-ray measurements. The DNA structure was monitored for 40 ns, and the distributions of the slide and z_p coordinates were obtained from the simulations. We find that all the double-stranded DNA (ds-DNA) strands transform from A- to B-DNA during the simulations. In addition, single-stranded DNAa (ss-DNAs) that are used to connect the ds-DNA to each surface are found to become adsorbed on the gold surfaces during this process, and the ds-DNAs bend (~143°) at their junctions with the two gold surfaces to accommodate the observed distance between gold surfaces using B-form DNA. We infer from this that the short length of DNA between the gold surfaces is not due to the presence of A-DNA.

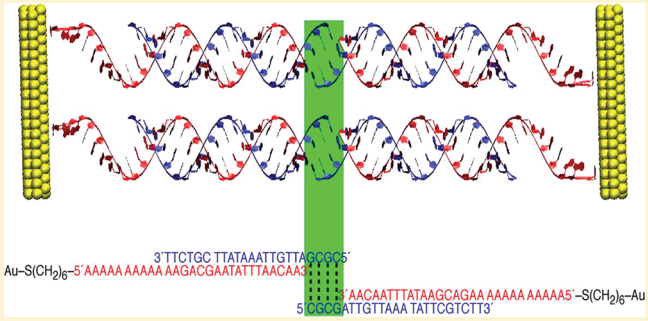

I. INTRODUCTION

Gel-like materials derived from DNA-linked gold nanoparticles (DNA-Au NPs) that have many unique optical, thermodynamic, and structural properties have emerged in the last 15 years as a result of advances in synthetic methods including the ability to routinely synthesize oligonucleotides with specified base pair sequences and the ability to chemically tether oligonucleotides to gold particles.[1−6] The hybridization between single-stranded DNA (ss-DNA) on different gold particles leads to linking of the particles into aggregates whose optical properties depend on the length of DNA, the size of the gold particles, and the density of DNAs on each particle. In addition, the thermal melting curves of the DNA-linked nanoparticle aggregates are unusually sharp.[7] Although the DNA-linked aggregates were initially found to have amorphous or even fractal structures,[8] in the past few years methods and DNA-sequences have been developed that enable the formation of superlattice crystals,[9] and a wide variety of crystal structures have been found based on simple design principles.[5]

Experiments have shown that functionalized gold nanoparticles can be used for DNA sensing applications. In particular, Mirkin and co-workers have exploited the optical properties of DNA-Au NPs to develop a highly selective colorimetric diagnostic method for DNA.[10,11] This diagnostic method relies on the distance dependent optical properties of gold particles, as it is well-known that the plasmon frequency of a collection of gold particles can be controlled by adjusting the distance between discrete nanoparticles.[12−18] This effect makes it important to understand what determines the structure of DNA in these materials; however, this structure, and particularly the length of DNA, is surprisingly different from what might be expected based on the usual Watson−Crick structure.[19] In particular, Hill et al.[20] and Park et al.[9] have reported that the length of DNA that links gold nanoparticles arranged in face-centered cubic or body-centered cubic structures is considerably shorter than the usual 3.4 Å rise per base-pair in Watson−Crick B-form DNA. Instead, it is comparable with the length of A-form DNA (~2.6 Å rise per base-pair[21]).

Most DNAs in nature adopt the B-form structure under standard buffer conditions or in vivo. Other forms of DNA usually exist under unusual conditions such as nonaqueous solvents, or as a transient structure, but the more compact A-DNA is thought to play a crucial role in gene expression.[22−24] Compared to B-DNA, A-form DNA is a larger diameter right-handed spiral with a wide and shallow minor groove, and a narrower and deeper major groove. The energy difference between A- and B-DNA is not large and can be overcome at room temperature by changing water activity, so previous studies have attempted to study the A ↔ B transition of DNA, from both experimental and computational aspects.[25−28] The mechanism of the A ↔ B transition is still elusive, but hydration[25] and electrostatics[28] are thought to be driving factors. A-form DNA exposes more hydrophobic atoms at the minor groove than B-form DNA does, and can be more stable at low water activity. Such low water activity can be brought about by either drying (reducing the number of water

Special Issue: Harold A. Scheraga Festschrift

Received: January 26, 2012
Revised: March 13, 2012
Published: March 16, 2012

   dx.doi.org/10.1021/jp300877e | J. Phys. Chem. B 2012, 116, 7000−7005

molecules) or mixing with other solvents such as ethanol. In addition, counterions will accumulate in the major groove and stabilize the phosphate-bridge water molecule more prominently in A-DNA than in B-DNA, barring sequence-dependent exceptions. On the other hand, electrostatic effects are more sensitive and favor different conformations at different ion concentrations. These two effects make the A ↔ B equilibrium very sensitive to the environment. In the case of the DNA-Au NPs, the DNAs that link nanoparticles are in very high concentration due to the high loading of DNA that can be achieved on gold particles[29] and the multiple DNAs that link each pair of nanoparticles. This makes counterion concentrations sufficiently large that osmotic effects dictate the minimum spacing between DNAs.[30] The influence of these factors on DNA length is unknown, although even for B-form DNA in solution, high salt can influence persistence length and therefore the flexibility of DNA's that link the two gold surfaces.[31]

The ability of classical force fields and molecular dynamics (MD) methods to describe the A ↔ B transition has been considered on numerous occasions in past work,[32−36] as it is a relevant parameter to the parametrization of force fields for describing DNA structures.[37] Both the CHARMM and AMBER force fields have been considered, and both are able to describe the preferential stability of B-DNA in water at low salt and the stability of A-DNA in ethanol/water solutions. In addition, one study demonstrated that the potential of mean force has no local minima between the A and B forms.[32] The AMBER force field has been used to show that A-DNA is stabilized relative to B-DNA by increasing salt,[35,36] but in the absence of nonaqueous solvent it is not clear from the calculations that there is an B → A transition as salt concentration increases, and experimental studies of added salt effects point toward a B → Z transition, where Z-DNA has a larger rise per base-pair than B-DNA.[38]

In this paper, we report the structural properties of DNA that link gold surfaces using MD simulations at the atomistic level, with emphasis on the stability of A-form DNA structures under circumstances where the 2.6 Å rise per base-pair is found. To model the high concentration of DNA found in the DNA-linked structures (and therefore the high counterion concentration), four ss-DNAs are attached to a [111] gold surface using a six-carbon alkylthiolate tether, and a complementary ss-DNA is introduced to form a double-stranded DNA (ds-DNA; Figure 1). The introduced ss-DNA also contains a four base linker (5′-CGCG), and this linker forms a ds-DNA upon hybridization with its counterpart from the other gold surface. The initial distance between the two gold surfaces is constrained to match that found in the experiments, so that we can study the effect of this constraint on the A → B transition. During the simulation, we monitor several structural parameters including the slide and z_p variables of DNA,[39] the angle between different portions of the ds-DNA, and the position of the adenines of ss-DNA.

II. COMPUTATIONAL DETAILS

A portion of the self-assembled DNA-Au NP structure in Figure 1A is modeled as shown in Figure 1B−D. For simulation of the system within a reasonable computational time scale, only the part shown in the black square in Figure 1 A is modeled. The gold substrate is chosen to be a flat surface (thereby modeling results either for the flat surfaces of gold prisms,[40] or for spherical particles that are sufficiently large)

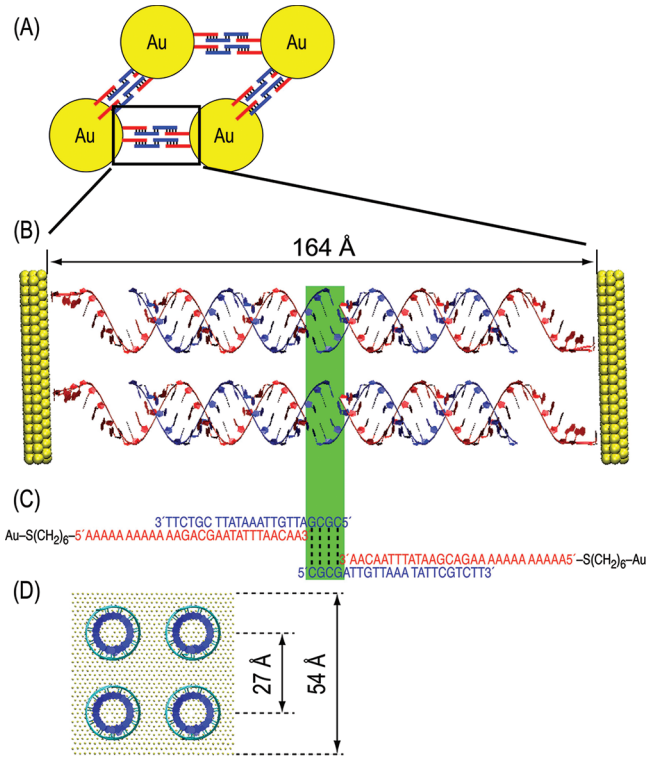

Figure 1. (A) Schematic representation of DNA-Au NPs. (B) DNA strands between gold particles shown in the black box in panel A are modeled at the atomistic level. Four DNA strands were used to connect two gold surfaces. The distance between the axes of neighboring DNA is 27 Å. (C) Sequence of DNA used for the simulation. Each of ss-DNA is linked to the center of the [111] surface of the gold surface using the $-S(CH_2)_6$ group. Dotted lines are used for the description of hydrogen bonding between linkers. The CGCG linker is highlighted by the green background. (D) Top view of four DNA strands between gold surfaces.

with dimensions 54 Å × 54 Å × 5 Å with the [111] surface taken to be at the top and bottom of the 5 Å thick layer. Four ss-DNAs (5′-AAAAA AAAAA AAGAC GAATA TTTAA CAA-3′) (a sequence that matches that used in the experiments) are attached to the [111] surface using a six-carbon alkylthiolate linker. A complementary ss-DNA (3′-TTCTG CTTAT AAATT GTTAG CGC-5′) is hybridized to the first ss-DNA so that part of this structure is double-stranded. This second ss-DNA also contains a 5′-CGCG sequence that acts as a dangling end. Another surface-bound ss-DNA and its complementary ss-DNA is developed, and a double helix is formed by hybridization of the dangling ends (5′-CGCG). The initial helical parameters of the ds-DNAs are adapted from the canonical A-DNA structure. Between the double helix and the dangling end, a nonbinding single DNA adenine base, called a flexor,[9] is added. This starting structure is developed using the x-leap module implemented in the AMBER package.[41] Even though the rotational registrations of four ds-DNA helices are identical (Figure 1 D), each ds-DNA is freely rotatable along the DNA axis.

The DNA sequence used here is taken from experiment,[9,20] and the distance between the two surfaces is taken to be 164 Å. This is the experimentally measured distance, and it is also the distance appropriate for the equilibrium structure of the A-form DNA if we assume that even the single-stranded portions are A-form. The distance between the DNA axes is taken to be 27 Å,

dx.doi.org/10.1021/jp300877e | J. Phys. Chem. B 2012, 116, 7000−7005

which is comparable to the experimental value for small (~10 nm) gold particles.[42] The maximum density of ss-DNA attached to gold nanoparticles is higher for particles with a smaller radius of curvature than for those with a larger radius of curvature, corresponding to a mean separation of 27 Å for 10 nm diameter nanoparticles, and increasing to 39 Å for 200 nm nanoparticles, or flat surfaces. Hurst et al. have proposed that a driving force for this density change is the splaying of the DNAs that occurs for small particles, as this reduces repulsions between the phosphates on the DNAs.[40] In our previous simulations, we obtained separations comparable to those seen in the experiments, and we found that it is an osmotic pressure rather than direct repulsions between phosphates that determines this separation.[43] In the present calculations, we have used the 27 Å separation so as to simulate the physical situation for small gold particles where there is a higher counterion density. However, we note that the unusually short DNA length arises both for small particles and for nanoscale gold prisms, which are essentially flat.[44] In the prism experiments, Millstone et al. found that the rise per DNA is ~2.8 Å, which is a comparable value to that for spherical gold nanoparticles even though the distance between the axes of the DNAs is ~38 Å.[6] Therefore, the distance between the DNA axes does not appear to affect the DNA conformation.

The system was solvated in a water box of 54 × 54 × 160 Å^3 using the SOLVATE module implemented in VMD,[45,46] and periodic boundary conditions are applied to the calculations. This box was filled with 12768 water molecules based on the modified TIP3P potential.[47,48] To neutralize the system, 400 Na^+ ions are added. The concentration of sodium ion is 1.4 M, which is comparable to that used in our previous simulation of ds-DNAs on a gold surface.[43]

The interactions between the gold atoms are described by Lennard-Jones potentials where the parameters (r = 2.951 Å and ε = 5.29 kcal/mol) are taken from the literature.[49] The force field parameters for the alkylthiolate are taken from the work of Hautman et al.,[50] while the parameters for DNA are taken from CHARMm.[51]

MD simulations were carried out using NAMD2.[52] A 1 ns MD simulation at 300 K with an NVT ensemble was performed to equilibrate the system. In the production period, the system was simulated for 40 ns using the NVT ensemble and Langevin dynamics at a temperature of 300 K with a damping coefficient γ = 5 ps^{-1}.[53] During the equilibration and production, the position of the gold atoms is fixed with harmonic constraints. Full electrostatics was employed using the particle-mesh Ewald method with a 1 Å grid width.[54] Nonbonded interactions were calculated using a group-based cutoff with a switching function and were updated every 5 time steps. Covalent bonds involving hydrogen were held rigid using the SHAKE algorithm,[55] allowing a 2 fs time step. Atomic coordinates were saved every 10 ps for the trajectory analysis. Two independent simulations were done, and the results were very similar, so only the results of one of the simulations are presented.

III. RESULTS AND DISCUSSION

A given DNA structure obtained by crystallography or MD simulation usually does not match all the classic criteria of either A- or B-DNA, but the average coordinate values fall in characteristic parameter ranges. However, the difference between canonical A- and B-DNA can be characterized by many conformational parameters, including the phase angle of sugar puckering, the glycosyl torsion between sugar and base, and the major and minor groove widths. Berman et al. suggested that the slide of neighboring bases (see the inset of Figure 2 A) is the most reliable parameter for discriminating A- and B-DNA obtained from the crystallography.[56] El Hassan et al. have suggested another parameter z_p, the mean z-coordinate of the backbone phosphorus atoms with respect to individual dimer reference frames (see the inset of Figure 2B), for discriminating A- and B-DNA.[57] For the structural analysis of our simulation, therefore, the values of slide and z_p are monitored during the simulation.

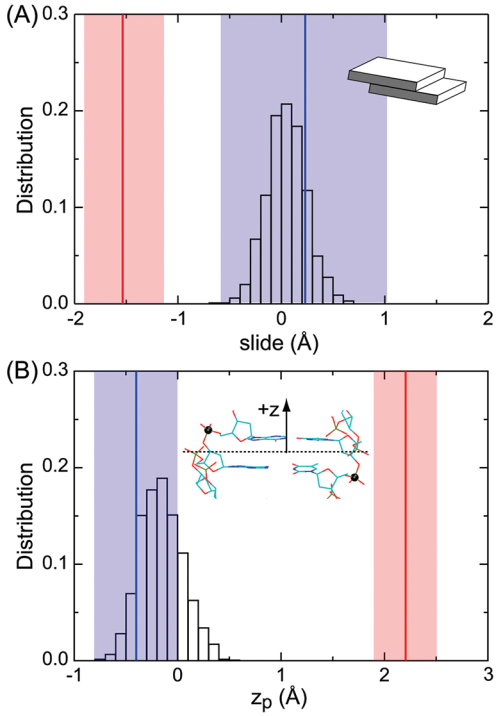

Figure 2. Distribution of (A) the slide and (B) z_p of ds-DNA during the last 10 ns of MD simulation. Average values and distribution of the slide and z_p of B-DNA found in the crystallographic data are shown in blue, whereas those of A-DNA are shown in red. Schematic definition of the slide and z_p is in the inset.

The distribution of the slide variable for ds-DNA during the last 10 ns of the MD simulation is shown in Figure 2A. Average values of the slide for A- (−1.53 ± 0.34 Å) and B-DNA (0.23 ± 0.81 Å) as obtained from crystallographic data are also shown for comparison. The slide variable obtained from our simulations (0.05 ± 0.19 Å (mean ±1σ)) is consistent with that of B-DNA. The distribution of z_p for ds-DNA obtained from our simulations is shown with the average values of A- (2.2 ± 0.3 Å) and B-DNA (−0.4 ± 0.4 Å) from crystallographic data in Figure 2B. The value of z_p obtained from the simulations (−0.15 ± 0.21 Å) is also consistent with that of B-DNA. It is well-known that G·C blocks exhibit A-DNA properties in solutions of low water activity, whereas the A·T blocks retain the B-DNA character in aqueous solution.[58−61] Since the ratio of G·C to A·T blocks in our ds-DNA structures is 4:14, the transition from A- to B-DNA observed in our simulation is consistent with this composition tendency. Calculations we have done with other sequences in which the ratio of G·C to A·T was varied show changes in slide and z_p that are consistent with expectations but with B-DNA always being dominant.

dx.doi.org/10.1021/jp300877e | J. Phys. Chem. B 2012, 116, 7000−7005

Snapshots of the system at 10 ns intervals during the simulation are shown in Figure 3. The alkylthiolate and ss-DNAs become adsorbed on the gold surface, and bending is observed in the linker region in all of the strands. This is consistent with our previous simulation of DNA between gold surfaces where the starting conformation of ds-DNA was B-DNA; it was observed that ss-DNA and the alkylthiolate was adsorbed on the gold surfaces, and the bending was observed in the linker region while the ds-DNA maintained a B-DNA conformation.

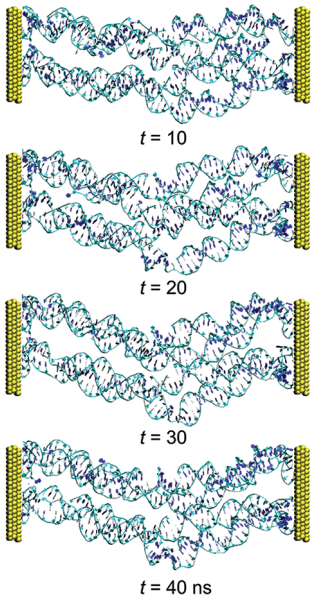

Figure 3. Snapshots of the MD simulation trajectory with the time interval of 10 ns.

In the present calculation, we also observed the bending of DNA at the linker region boundary where the principal axis of ds-DNA was used for measuring the angle (θ) between ds-DNAs. The calculated average value of θ was 143° ± 13° during the last 10 ns of simulation (Figure 4). From this, we could conclude that the bending of DNA at the linker region boundary occurs irrespective of the starting structure of ds-DNA. The adenine (flexor) inserted between the linker and ds-DNA serves as the focal point for bending because this adenine is not complemented with a nucleobase in the complementary strand. Park et al. also reported that the flexor with greater flexibility enhances the assembly of DNA-functionalized gold nanoparticles and results in a well-defined crystalline structure. This bending of DNA at the flexor was also reported in our previous paper,[19] where we simulated a ds-DNA between gold surfaces with an assumed B-form DNA initial structure. During the simulation, the distance between gold surfaces was slowly changed from 233 Å to 163 Å, and it was found that ds-DNA maintained a B-DNA conformation throughout, with all base-pair hydrogen bonds remaining intact. We also observed, both in the present results and in previous studies, the adsorption of ss-DNA and of the alkylthiolate tether on the gold surfaces during the simulation. As seen in Figure 3, the ss-DNAs begin to adsorb on the gold surface at an early stage of the simulation. The distribution of adenines along the distance from the gold surface is shown in Figure 5A. Most of adenines of the ss-DNA region are found within 20 Å from the gold surface, and the highest peak positions are around 10 Å away from the gold surface. As shown in Figure 5B, most of adenines in ss-DNA are parallel to the gold surface.

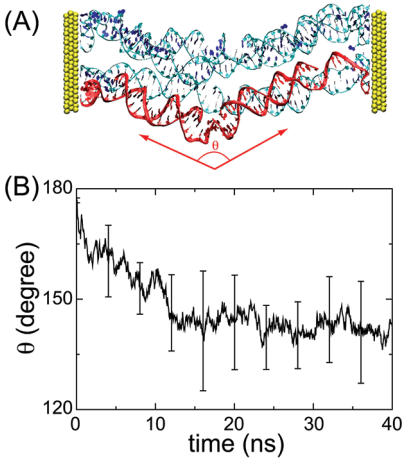

Figure 4. (A) The angle between two ds-DNAs (θ) linked by the CGCG sequence is defined by the principal axis of each ds-DNA. One strand of DNA is highlighted in red to show how θ is defined. (B) Fluctuation of θ along the MD simulation. The average value of θ during the last 10 ns of four DNAs is 143°.

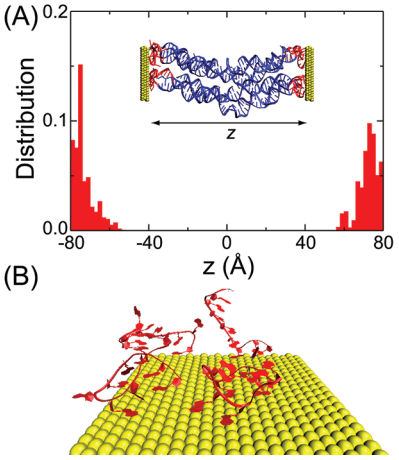

Figure 5. (A) Distribution of the base of ADE_{10} linker along the z-axis. Snapshot of the system is in the inset, where the ADE_{10} linker is modeled in red. Most of the ADE_{10} is in the vicinity of the gold surfaces. (B) Snapshot of ADE_{10} on the gold surface.

IV. CONCLUSION

We have observed the structures of ds-DNAs that link two gold surfaces using MD simulations for 40 ns at the atomistic level. On the basis of the distribution of the slide and z_p of DNA, we concluded that ds-DNAs adopt a B-form DNA conformation when linking two gold surfaces. This indicates that neither the high salt environment associated with the DNA-Au NP structures nor the mechanical constraints imposed by the distance between the two gold surfaces is sufficient to stabilize the A-form. In addition, we also found the bending of ds-DNAs at their junctions and the adsorption of ss-DNA on the gold surfaces serve to accommodate the nominal 2.6 Å per base-pair distance between gold surfaces with B-form DNA without leading to dehybridized base-pairs. This result agrees with our earlier calculations[19] where the DNA was taken to be in the B-

dx.doi.org/10.1021/jp300877e | J. Phys. Chem. B 2012, 116, 7000−7005

form, thus showing that the final structure is independent of the starting point of the simulation used to generate the short DNA-length.

The computational approach used in this report shows the value of an atomistic model for describing DNA-Au NPs even though an alternative approach such as a coarse-grained model would be needed for modeling the larger scale structures that are involved in DNA-linked nanocrystals.[62,63] This work also suggests that a new form of DNA-Au NP materials might be achievable if the A-form can be stabilized, presumably by lowering water activity.

AUTHOR INFORMATION

Corresponding Author

*Electronic mail: schatz@chem.northwestern.edu. Phone: (847) 491-5657. Fax: (847) 491-7713.

Notes

The authors declare no competing financial interest.

ACKNOWLEDGMENTS

This research was supported by the National Science Foundation (Grant CHE-0843832), by the NSEC Center at Northwestern (NSF Grant EEC-0647560), and by AFOSR MURI Grant FA9550-11-1-0275.

REFERENCES

(1) Alivisatos, A. P.; Johnsson, K. P.; Peng, X. G.; Wilson, T. E.; Loweth, C. J.; Bruchez, M. P.; Schultz, P. G. *Nature* **1996**, *382*, 609.
(2) Mirkin, C. A.; Letsinger, R. L.; Mucic, R. C.; Storhoff, J. J. *Nature* **1996**, *382*, 607.
(3) Lee, O. S.; Prytkova, T. R.; Schatz, G. C. *J. Phys. Chem. Lett.* **2010**, *1*, 1781.
(4) Prigodich, A. E.; Lee, O. S.; Daniel, W. L.; Seferos, D. S.; Schatz, G. C.; Mirkin, C. A. *J. Am. Chem. Soc.* **2010**, *132*, 10638.
(5) Macfarlane, R. J.; Lee, B.; Jones, M. R.; Harris, N.; Schatz, G. C.; Mirkin, C. A. *Science* **2011**, *334*, 204.
(6) Jones, M. R.; Macfarlane, R. J.; Lee, B.; Zhang, J. A.; Young, K. L.; Senesi, A. J.; Mirkin, C. A. *Nat. Mater.* **2010**, *9*, 913.
(7) Jin, R.; Wu, G.; Li, Z.; Mirkin, C. A.; Schatz, G. C. *J. Am. Chem. Soc.* **2003**, *125*, 1643.
(8) Park, S. Y.; Lee, J. S.; Georganopoulou, D.; Mirkin, C. A.; Schatz, G. C. *J. Phys. Chem. B* **2006**, *110*, 12673.
(9) Park, S. Y.; Lytton-Jean, A. K. R.; Lee, B.; Weigand, S.; Schatz, G. C.; Mirkin, C. A. *Nature* **2008**, *451*, 553.
(10) Elghanian, R.; Storhoff, J. J.; Mucic, R. C.; Letsinger, R. L.; Mirkin, C. A. *Science* **1997**, *277*, 1078.
(11) Storhoff, J. J.; Elghanian, R.; Mucic, R. C.; Mirkin, C. A.; Letsinger, R. L. *J. Am. Chem. Soc.* **1998**, *120*, 1959.
(12) Brust, M.; Bethell, D.; Schiffrin, D. J.; Kiely, C. J. *Adv. Mater.* **1995**, *7*, 795.
(13) Freeman, R. G.; Grabar, K. C.; Allison, K. J.; Bright, R. M.; Davis, J. A.; Guthrie, A. P.; Hommer, M. B.; Jackson, M. A.; Smith, P. C.; Walter, D. G.; Natan, M. J. *Science* **1995**, *267*, 1629.
(14) Heath, J. R.; Knobler, C. M.; Leff, D. V. *J. Phys. Chem. B* **1997**, *101*, 189.
(15) Lin, X. M.; Wang, G. M.; Sorensen, C. M.; Klabunde, K. J. *J. Phys. Chem. B* **1999**, *103*, 5488.
(16) Pileni, M. P. *New J. Chem.* **1998**, *22*, 693.
(17) Schmucker, A. L.; Harris, N.; Banholzer, M. J.; Blaber, M. G.; Osberg, K. D.; Schatz, G. C.; Mirkin, C. A. *ACS Nano* **2010**, *4*, 5453.
(18) Storhoff, J. J.; Lazarides, A. A.; Mucic, R. C.; Mirkin, C. A.; Letsinger, R. L.; Schatz, G. C. *J. Am. Chem. Soc.* **2000**, *122*, 4640.
(19) Lee, O. S.; Schatz, G. C. *J. Comput. Theor. Nanosci.* **2010**, *7*, 2568.
(20) Hill, H. D.; Macfarlane, R. J.; Senesi, A. J.; Lee, B.; Park, S. Y.; Mirkin, C. A. *Nano Lett.* **2008**, *8*, 2341.
(21) Charney, E.; Chen, H. H.; Rau, D. C. *J. Biomol. Struct. Dyn.* **1991**, *9*, 353.
(22) Ivanov, V. I.; Minchenkova, L. E. *Mol. Biol.* **1994**, *28*, 780.
(23) GuzikevichGuerstein, G.; Shakked, Z. *Nat. Struct. Biol.* **1996**, *3*, 32.
(24) Pardo, L.; Pastor, N.; Weinstein, H. *Biophys. J.* **1998**, *75*, 2411.
(25) Mazur, A. K. *J. Am. Chem. Soc.* **2003**, *125*, 7849.
(26) Mazur, A. K. *J. Chem. Theory Comput.* **2005**, *1*, 325.
(27) Mazur, A. K. *ChemPhysChem* **2008**, *9*, 2691.
(28) Rudd, L.; Lee, D. J.; Kornyshev, A. A. *J. Phys.: Condens. Matter* **2007**, *19*, 416103.
(29) Hill, H. D.; Millstone, J. E.; Banholzer, M. J.; Mirkin, C. A. *ACS Nano* **2009**, *3*, 418.
(30) Lee, J.-S.; Seferos, D. S.; Giljohann, D. A.; Mirkin, C. A. *J. Am. Chem. Soc.* **2008**, *130*, 5430.
(31) Porschke, D. *Biophys. Chem.* **1991**, *40*, 169.
(32) Banavali, N. K.; Roux, B. *J. Am. Chem. Soc.* **2005**, *127*, 6866.
(33) Jayaram, B.; Sprous, D.; Young, M. A.; Beveridge, D. L. *J. Am. Chem. Soc.* **1998**, *120*, 10629.
(34) Knee, K. M.; Dixit, S. B.; Aitken, C. E.; Ponomarev, S.; Beveridge, D. L.; Mukerji, I. *Biophys. J.* **2008**, *95*, 257.
(35) Sprous, D.; Young, M. A.; Beveridge, D. L. *J. Phys. Chem. B* **1998**, *102*, 4658.
(36) Srinivasan, J.; Cheatham, T. E.; Cieplak, P.; Kollman, P. A.; Case, D. A. *J. Am. Chem. Soc.* **1998**, *120*, 9401.
(37) MacKerell, A. D.; Banavali, N. K. *J. Comput. Chem.* **2000**, *21*, 105.
(38) Reich, Z.; Friedman, P.; Scolnik, Y.; Sussman, J. L.; Minsky, A. *Biochemistry* **1993**, *32*, 2116.
(39) Lu, X. J.; Shakked, Z.; Olson, W. K. *J. Mol. Biol.* **2000**, *300*, 819.
(40) Hurst, S. J.; Hill, H. D.; Macfarlane, R. J.; Wu, J. S.; Dravid, V. P.; Mirkin, C. A. *Small* **2009**, *5*, 2156.
(41) Pearlman, D. A.; Case, D. A.; Caldwell, J. W.; Ross, W. S.; Cheatham, T. E.; Debolt, S.; Ferguson, D.; Seibel, G.; Kollman, P. *Comput. Phys. Commun.* **1995**, *91*, 1.
(42) Hurst, S. J.; Lytton-Jean, A. K. R.; Mirkin, C. A. *Anal. Chem.* **2006**, *78*, 8313.
(43) Lee, O.-S.; Schatz, G. C. *J. Phys. Chem. C* **2009**, *113*, 15941.
(44) Millstone, J. E.; Georganopoulou, D. G.; Xu, X. Y.; Wei, W.; Li, S. Y.; Mirkin, C. A. *Small* **2008**, *4*, 2176.
(45) Grubmuller, H. *VMD*, version 1.2; Theoretical Biophysics Group, Institute for Medical Optics, Ludwig-Maximilian University: Munich, 1996.
(46) Humphrey, W.; Dalke, A.; Schulten, K. *J. Mol. Graphics* **1996**, *14*, 33.
(47) Jorgensen, W. L.; Chandrasekhar, J.; Madura, J. D.; Impey, R. W.; Klein, M. L. *J. Chem. Phys.* **1983**, *79*, 926.
(48) Mackerell, A. D.; Wiorkewiczkuczera, J.; Karplus, M. *J. Am. Chem. Soc.* **1995**, *117*, 11946.
(49) Heinz, H.; Vaia, R. A.; Farmer, B. L.; Naik, R. R. *J. Phys. Chem. C* **2008**, *112*, 17281.
(50) Hautman, J.; Klein, M. L. *J. Chem. Phys.* **1989**, *91*, 4994.
(51) MacKerell, A. D.; et al. *J. Phys. Chem. B* **1998**, *102*, 3586.
(52) Kale, L.; Skeel, R.; Bhandarkar, M.; Brunner, R.; Gursoy, A.; Krawetz, N.; Phillips, J.; Shinozaki, A.; Varadarajan, K.; Schulten, K. *J. Comput. Phys.* **1999**, *151*, 283.
(53) Martyna, G. J.; Tobias, D. J.; Klein, M. L. *J. Chem. Phys.* **1994**, *101*, 4177.
(54) Darden, T.; York, D.; Pedersen, L. *J. Chem. Phys.* **1993**, *98*, 10089.
(55) Andersen, H. C. *J. Comput. Phys.* **1983**, *52*, 24.
(56) Berman, H. M.; Olson, W. K.; Beveridge, D. L.; Westbrook, J.; Gelbin, A.; Demeny, T.; Hsieh, S. H.; Srinivasan, A. R.; Schneider, B. *Biophys. J.* **1992**, *63*, 751.
(57) El Hassan, M. A.; Calladine, C. R. *Philos. Trans. R. Soc. London, Ser. A* **1997**, *355*, 43.
(58) Burd, J. F.; Wartell, R. M.; Dodgson, J. B.; Wells, R. D. *J. Biol. Chem.* **1975**, *250*, 5109.

(59) Early, T. A.; Kearns, D. R.; Burd, J. F.; Larson, J. E.; Wells, R. D. *Biochemistry* **1977**, *16*, 541.
(60) Wang, Y.; Thomas, G. A.; Peticolas, W. L. *J. Biomol. Struct. Dyn.* **1987**, *5*, 249.
(61) Wang, Y.; Thomas, G. A.; Peticolas, W. L. *J. Biomol. Struct. Dyn.* **1989**, *6*, 1177.
(62) Maciejczyk, M.; Spasic, A.; Liwo, A.; Scheraga, H. A. *J. Comput. Chem.* **2010**, *31*, 1644.
(63) Knotts, T. A.; Rathore, N.; Schwartz, D. C.; de Pablo, J. J. *J. Chem. Phys.* **2007**, 126.